A Two-Parameter Framework to Describe Effects of Constraint Loss on Cleavage Fracture and Implications for Failure Assessments of Cracked Components

S. Cravero and C. Ruggieri
Dept. of Naval Architect. and Ocean Engineering
University of São Paulo – PNV – EPUSP
05508-900 São Paulo, SP. Brazil
sebastian.cravero@poli.usp.br and
claudio.ruggieri@poli.usp.br

This study builds upon the J-Q approach to characterize constraint effects on cleavage fracture behavior of cracked structural components. Discussions emphasize features of current two-parameter fracture methodologies which extend the limits of applicability of single parameter fracture approaches when LSY effects prevail. Inclusion of the second parameter (Q) in failure assessment procedures leads to the construction of experimentally derived fracture toughness loci, rather than conventional, single-valued definitions of toughness. The plan of the article is as follows. First, the notion of crack tip constraint and its connection with SSY reference fields is introduced. This is followed by a brief description of the J-Q theory to define the hydrostatic parameter Q. The paper then addresses representative numerical solutions which provide J-Q trajectories for common fracture specimens under bend and tensile loading, including deep and shallow crack SE(B) and SE(T) specimens. These analyses, when taken together with previous works, provide a fairly extensive body of results against which the robustness of the J-Q methodology can be weighed.
***Keywords**: Cleavage fracture, crack-tip constraint, Q-parameter, J-Integral, finite elements*

Introduction

Conventional fracture mechanics methodologies to assess unstable cracking behavior (cleavage fracture) of different cracked bodies (*i.e.*, laboratory specimens and engineering structures) rely on the similarity of their respective crack tip stress and deformation fields. Under well-contained near-tip plasticity, a single parameter, such as the linear elastic stress intensity factor, K, and the J-integral (or, equivalently, the corresponding value of the crack tip opening displacement - CTOD or δ), uniquely scales the elastic-plastic near-tip fields (Hutchinson, 1983). To the extent that such one-parameter singular fields dominate over microstructuraly significant size scales (*i.e.*, the fracture process zone of a few CTODs ahead of a macroscopic crack), parameters K and J (δ) fully describe the local conditions leading to unstable (cleavage) failure. However, fracture testing of ferritic structural steels in the ductile-to-brittle transition (DBT) region consistently reveals a significant effect of specimen geometry, loading mode (bending *vs.* tension) and strain hardening on measured cleavage toughness values (see Sorem et al. (1991), Joyce and Link (1997), Ruggieri and Dodds (1996) for illustrative data). Figure 1 provides toughness data for a typical high strength structural steel tested in the DBT region (Ruggieri and Dodds, 1996) which clearly shows significant elevations in the measured values of cleavage fracture toughness, J_c, for shallow crack SE(B) specimens. This apparent increased toughness of structural steels in service conditions has enormous practical implications in defect assessment procedures, particularly repair decisions and life extension programs of in-service structures.

The marked differences of J_c-values for shallow crack and deep crack specimen geometries exhibited by the plots shown in Fig. 1 reflect the loss of one-to-one correspondence between J and the elastic-plastic crack-tip fields. When extensive plastic deformation develops ahead of the crack tip, the interaction of crack-tip plastic zones with nearby traction-free surfaces and with global plastic zones affects strongly the near tip strain-stress fields. Stresses relax below the values determined uniquely by the J-integral for the high constraint condition of small-scale yielding (SSY) which exists early in the loading of cracked bodies. This loss of a unique relationship between the crack-tip fields and J underlies the constraint loss phenomenon which plays a dominant role in the observed specimen geometry and loading mode effects on measured cleavage toughness values. These effects are most pronounced for low-to-medium strength structural steels operating in the DBT region where stress-controlled cleavage mechanisms dominate.

The above arguments that a single parameter might not suffice to characterize the near-tip behavior of cracked geometries under large-scale yielding (LSY) conditions motivated the development of two-parameter fracture theories. Under fixed loading, such methodologies assume a separable form for the actual cracked-body fields in a high triaxiality field (such as the SSY field) and a constant field which quantifies the level of crack tip stress triaxiality. These research efforts proceeded along essentially two lines: (1) the J-T methodology developed by Hancock and co-workers (Al-Ani and Hancock,1991; Betegon and Hancock, 1991; Du and Hancock, 1991), Parks (1992) and Wang (1993) building upon the elastic T-stress, and (2) the J-Q methodology developed by O'Dowd and Shih (1991, 1992) building upon the hydrostatic parameter Q. Both frameworks characterize families of self-similar fields which describe crack tip fracture states in the full range of high and low triaxiality. Within these methodologies, J sets the size scale over which large stresses and strain develop while the second parameter (T or Q) scales the near-tip distribution relative to the reference stress state. While the J-T and J-Q approaches are essentially equivalent under well-contained near-tip plastic deformation, the elastic T-stress become undefined under fully-yielded conditions as the elastic near-tip fields upon which T is derived no longer apply. In contrast, the Q-parameter continues to characterize the evolution of near-tip stress triaxiality over a wider range of crack-tip plasticity associated with a wide variety of crack configurations under general loading conditions.

Paper accepted October, 2003. Technical Editor: Edgar Nobuo Mamiya.

This study builds upon the *J-Q* approach to characterize constraint effects on cleavage fracture behavior of cracked structural components. Discussions emphasize features of current two-parameter fracture methodologies which extend the limits of applicability of single parameter fracture approaches when LSY effects prevail. Inclusion of the second parameter (*Q*) in failure assessment procedures leads to the construction of experimentally derived fracture toughness loci, rather than conventional, single-valued definitions of toughness. The plan of the article is as follows. The next section introduces the notion of crack tip constraint and its connection with SSY reference fields. This is followed by a brief description of the *J-Q* theory to define the hydrostatic parameter *Q*. The paper then addresses representative numerical solutions which provide *J-Q* trajectories for common fracture specimens under bend and tensile loading, including deep and shallow crack SE(B) and SE(T) specimens. These analyses, when taken together with previous works, provide a fairly extensive body of results against which the robustness of the *J-Q* methodology can be weighed.

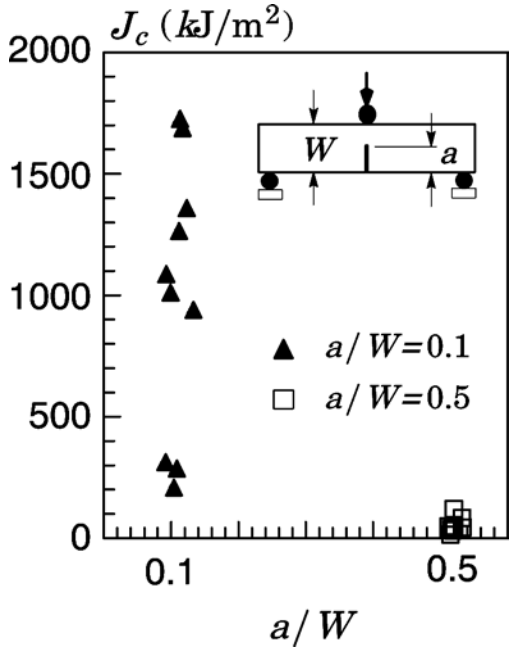

Figure 1. Toughness values (J_c) for a high strength structural steel measured in the DBT region using deep and shallow crack SE(B) specimens.

Two-Parameter Characterization: The J-Q Methodology

T-Stress and Reference Fields Under SSY Conditions

Constraint most generally refers to the evolving level of stress triaxiality ahead of the crack front under increased remote loading. A widely adopted approach to describe the levels of constraint which develop in (finite) cracked configurations upon increased loading employs full "reference" fields constructed for the high triaxiality SSY condition; fields computed for the finite body are compared to SSY fields to define relative constraint differences. Within this framework, the differences in the actual finite-body field and the reference SSY field quantify the extent of large scale yielding (LSY) that develops as deformation progresses. At increasing loads in the finite body, the initially strong SSY fields gradually diminish as crack-tip plastic zones increasingly merge with the global bending plasticity on the nearby traction free boundaries. The phenomenon of constraint loss requires larger *J*-values in the cracked configuration to generate a highly stressed region ahead of crack tip sufficient to trigger cleavage. Consequently, once SSY conditions no longer apply, the near-tip stresses (and strains) that develop ahead of a macroscopic crack cannot be described uniquely by *J* (or, equivalently, by *K* or CTOD).

The SSY fields are easily constructed from a modified boundary layer (MBL) formulation (Larsson and Carlsson, 1974) applied to a single-ended crack in an infinite body. Figure 2 shows the plane-strain finite element model for an infinite domain, single-ended crack problem with a initially blunted notch (finite root radius, ρ_0); Mode I loading of the far field permits analysis using one-half of the domain as shown. With the plastic region (here defined by its radius R_p) limited to a small fraction of the domain radius, $R_p<R/20$, the general form of the asymptotic crack-tip stress fields well outside the plastic region is given by the the first two terms of William's linear elastic solution (1957) in the form

$$\sigma_{ij} = \frac{K_{\rm I}}{\sqrt{2\pi\, r}} f_{ij}(\theta) + T\delta_{1i}\delta_{1j} \quad . \tag{1}$$

Here, r and θ are polar coordinates centered at the crack tip (see Fig. 2), $K_{\rm I}$ is the stress intensity factor, $f_{ij}(\theta)$ define the angular variations of in-plane stress components, and the non-singular term T represents a tension (or compression) stress parallel to the crack. Larsson and Carlsson (1974) have earlier demonstrated that this second term in the above Eq. (1), also denoted as *T*-stress - a term coined by Rice (1974), has a strong effect on the shape and size of the plastic zone as well as on crack tip fields of common 2D crack configurations. Setting T=0 recovers the asymptotic linear stress field for a symmetrically loaded Mode I crack as characterized solely by the stress intensity factor, K, which forms the basis of linear elastic fracture mechanics.

Crack tip fields differing in stress triaxiality can be generated by varying the levels of the non-singular stress T imposed on the model. Based upon dimensional considerations, these fields define a family of self-similar crack tip fields parameterized by T/σ_0 in the form

$$\sigma_{ij} = \sigma_0\, g_{ij}\left(\frac{r}{J/\sigma_0}, \theta, T/\sigma_0\right) \quad , \tag{2}$$

where

$$J = \frac{1-\nu^2}{E} K_{\rm I}^2 \tag{3}$$

for the MBL model under plane strain conditions; here, E is Young's modulus and ν is Poisson's ratio. As noted by Rice (1974), the *T*-stress does not affect the *J*-integral (or *K*) such that Equation (2) provides a rigorous two-parameter description of the linear elastic fields where parameter T/σ_0 quantifies the level of near-tip stress triaxiality under conditions of well-contained plasticity.

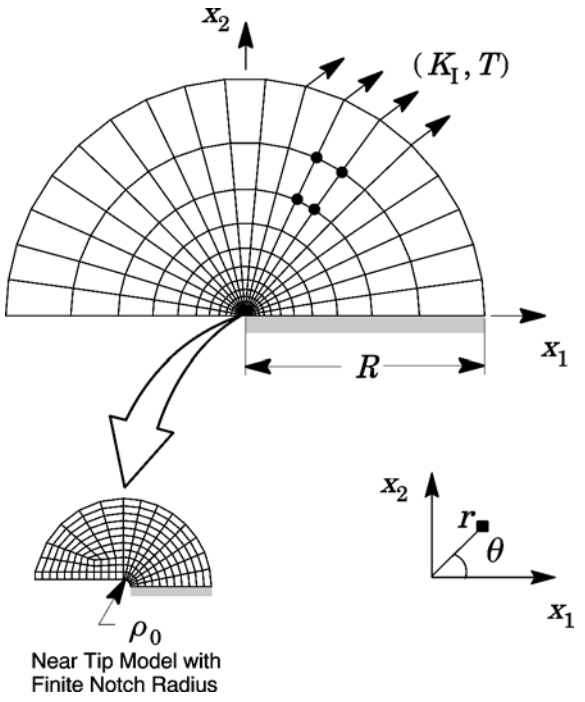

Figure 2. Modified boundary layer (MBL) model for an infinite domain, single-ended crack with a initially blunted notch and (*K*, *T*) fields imposed on the boundary.

Figure 3(a-d) provides the plane strain crack-tip fields resulting from the MBL model for well-contained, limited scale plasticity under varying levels of applied *T*-stress. These results have been obtained for an elastic-plastic material following the power hardening stress-strain response given by Eq. (8) with n=10 and E/σ_0=500 using large geometry changes (LCG) and incremental plasticity (Trovato and Ruggieri, 2001). In the plots, distances all scale with $(K_I/\sigma_0)^2$ whereas the opening stresses are normalized by σ_0. At very low remote loading for all levels of applied *T*-stress (K_I=20, 40 MPa×m$^{1/2}$), the near-tip stresses increase as the process of crack-tip blunting takes place. After the notch root radius increases to several times the initial radius, ρ_0, a *steady state solution* develops so that the near-tip fields under SSY conditions are simply a continuous series of self-similar states. Additional results for analyses conducted by Trovato and Ruggieri (2001) for materials with different elastic-plastic behavior display essentially similar trends. These plane-strain fields thus define a family of reference fields for stationary cracks where specified values for K_I and *T* uniquely define the elastic-plastic fields along the crack tip when a vanishingly small plastic zone encloses the tip.

Correlations of fracture conditions across different crack geometries/loading modes for the same material based upon the load parameter T/σ_0 have been conducted by Bilby et al. (1986), Betegon and Hancock (1991), Al-Ani and Hancock (1991) and Wang (1993). However, a major point of criticism to the *T*-stress approach as a broad descriptor of near-tip stress triaxiality for cracked configurations is that the elastic solution given by Eq. (1), upon which the *T*-stress is defined, is an asymptotic solution which is increasingly violated as plastic flow progresses beyond well-contained near-tip yielding. While numerical studies (Parks, 1992) have shown that the applicability of the *T*-stress as a correlator of near-tip stress triaxiality can be extended to LSY conditions for a variety of plane strain crack geometries and loadings, the theoretical deficiencies still remain as the elastic *T*-stress become undefined under fully yielded conditions. Nevertheless, the approach still provides a rational and tractable two-parameter description of the near-tip stress-strain fields under limited scale plasticity which proves valuable in characterizing the evolving levels of constraint for SSY conditions.

The *J-Q* Theory

The above limitations prompted researchers to consider multi-parameter descriptions of stationary crack tip fields applicable under large-scale yielding conditions. Li and Wang (1986), Sharma and Aravas (1991) constructed higher order asymptotic solutions for power law hardening materials based upon the HRR crack-tip stress and strain fields (Hutchinson, 1968; Rice and Rosengren, 1968). These results motivated O'Dowd and Shih (1991, 1992), hereafter O&S, to propose an approximate two-parameter description for the elastic-plastic crack tip fields based upon a triaxiality parameter more applicable under LSY conditions for materials with elastic-plastic response. Guided by detailed numerical analyses employing the MBL model previously described, O&S identified a family of self-similar fields in the form

$$\sigma_{ij} = \sigma_0 \, h_{ij}\left(\frac{r}{J/\sigma_0}, \theta, Q\right) \quad , \tag{4}$$

where the dimensionless second parameter *Q* defines the amount by which σ_{ij} in fracture specimens differ from the reference SSY solution with *T*=0. Here, the *J*-integral sets the size scale over which high stresses develop while the second parameter, *Q*, quantifies the level of stress triaxiality at distances of a few CTODS ahead of the crack tip; such dimension defines the physically relevant length scale of the (cleavage) fracture process zone.

Limiting attention to the forward sector ahead of the crack tip between the $SSY_{T=0}$ and the fracture specimen fields, O&S showed that *Q* corresponds effectively to a spatially uniform hydrostatic stress, *i.e.*, the difference field relative to a high triaxiality reference stress state in the form

$$\sigma_{ij} = \sigma_{ij}\Big|_{ssy;T=0} + Q\,\sigma_0\,\delta_{ij} \quad ; \quad |\theta| < \frac{\pi}{2} \; , \; \frac{J}{\sigma_0} < r < \frac{5J}{\sigma_0} \quad . \tag{5}$$

Operationally, *Q* is defined by

$$Q = \frac{\sigma_{\theta\theta} - \sigma_{\theta\theta}\big|_{SSY;T=0}}{\sigma_0} \quad , \quad \theta = 0 \, , \, r = \frac{2J}{\sigma_0} \tag{6}$$

where finite element analyses containing sufficient mesh refinement to resolve the fields at this length scale provide the finite body stresses $\sigma_{\theta\theta}$. Here, we note that *Q* is evaluated at $r=2(J/\sigma_0)$ for definiteness; this distance is outside the finite strain (blunting) region but still within the *J-Q* annulus. Construction of a *J-Q* trajectory follows by evaluation of Eq. (6) at each stage in loading of the finite body. This procedure imposes no restrictions on models to describe material flow properties, incremental *vs.* deformation plasticity or strain rate effects. Large geometry changes (LGC) may be included although values of *Q* derived from small geometry change (SGC) analyses prove satisfactory in applications which make use of stresses sufficiently outside the near tip blunting region ($r > J/\sigma_0$).

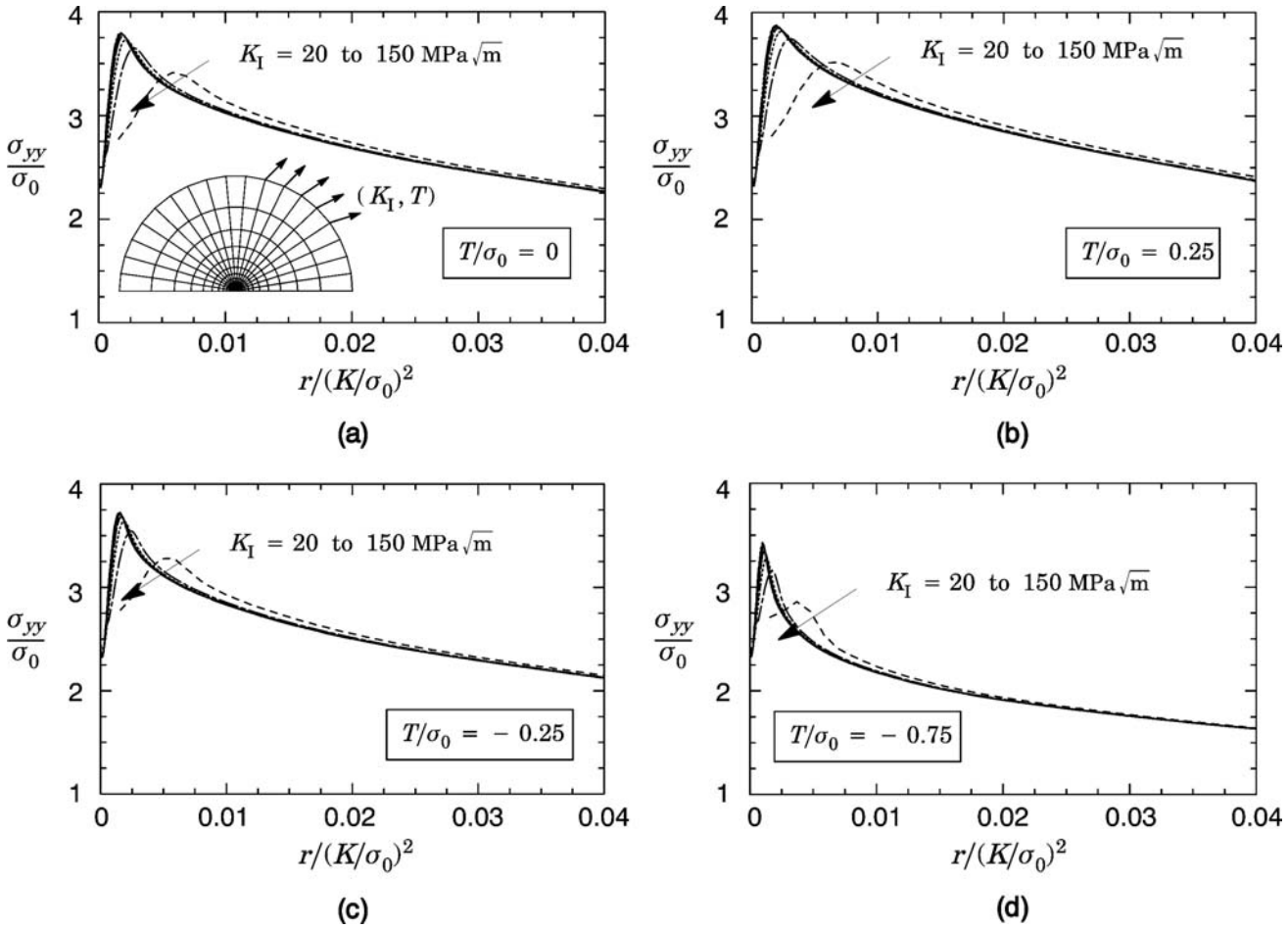

Figure 3. Near-tip stresses under *SSY* conditions for n=10, E/σ_0=500.

Computational Procedures

Finite Element Models

Plane-strain finite element analyses are conducted on conventional fracture specimens loaded predominantly in bending and tension. The matrix analysis includes a deeply cracked compact tension C(T) geometry with a/W=0.6 and shallow and deeply cracked SE(B), SE(T) and M(T) geometries with a/W=0.1 and 0.5. Here, a is the crack length and W is the specimen width. Figure 4 shows the geometry and specimen dimensions for the analyzed crack configurations. Figure 5 displays the finite element model constructed for the plane-strain analysis of the C(T) specimen with a/W=0.6. Simmetry conditions enable analyses using one-half of the plane-strain models for the C(T), SE(B) and SE(T) specimens and one-quarter of the plane-strain model for the M(T) specimen with appropriate constraints imposed on the symmetry planes. A focused ring of elements surrounding the crack front in the radial direction is used with a small key-hole at the crack tip; the radius of the key-hole, ρ_0, is 2.5×10^{-3}mm. This initial root radius at the crack front (blunt tip) avoids numerical problems with the computation of near-tip stresses and accelerates convergence of the plasticity algorithms during the initial stage of blunting. The half-symmetric model for the C(T) specimens has 2600 nodes and 1202 8-node, 3-D elements with plane-strain constraints imposed (w=0) on the nodes. The models for the SE(B), SE(T) and M(T) specimens have similar features and similar levels of mesh refinement.

Numerical analyses of the SSY model shown in Fig. 2 provide the reference stress fields needed to compute parameter Q. The numerical solutions for a stationary crack under well-defined SSY conditions (with the T-stress term in Eq. (1) set to zero, *i.e.*, T=0) are generated by imposing displacements of the elastic, Mode I singular field on the outer circular boundary (r=R) which encloses the crack

$$u(r,\theta) = K_I \frac{1+\nu}{E}\sqrt{\frac{r}{2\pi}}\cos\left(\frac{\theta}{2}\right)\left(3-4\nu-\cos\theta\right) \qquad (7)$$
$$v(r,\theta) = K_I \frac{1+\nu}{E}\sqrt{\frac{r}{2\pi}}\sin\left(\frac{\theta}{2}\right)\left(3-4\nu-\cos\theta\right)$$

where u and v are the displacements in the x_1 and x_2 direction respectively, r and θ are polar coordinates centered at the crack-tip with $\theta = 0$ corresponding to a line ahead of the crack tip, E is the Young's modulus and ν is Poisson's ratio. The SSY model has one thickness layer of 2065 8-node, 3-D elements with plane-strain constraints imposed (w=0) on the nodes. The crack tip region has the same mesh refinement as the fracture specimes with an initially blunted crack tip ($\rho_0 = 2.5\times10^{-3}$mm).

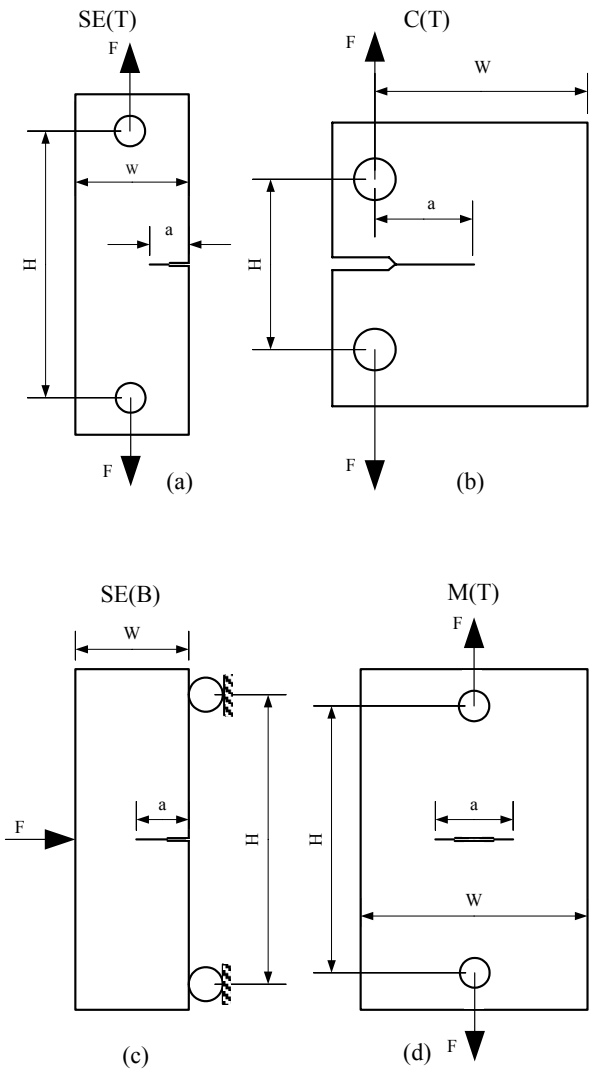

Figure 4. Geometry of fracture specimens employed in the analyses.

Constitutive Models

The elastic-plastic constitutive model employed in the present analyses follows a small strain J_2 flow theory with conventional Mises plasticity. The numerical solutions for the fracture specimens utilize a simple power-hardening model to characterize the uniaxial true stress-logarithmic strain in the form

$$\begin{aligned} \varepsilon/\varepsilon_0 &= \sigma/\sigma_0 \quad , \quad \varepsilon_0 \le \varepsilon \\ \varepsilon/\varepsilon_0 &= (\sigma/\sigma_0)^n \quad , \quad \varepsilon_0 > \varepsilon \end{aligned} \tag{8}$$

Here, n denotes the strain hardening exponent, σ_0 and ε_0 are the reference (yield) stress and strain, respectively. These finite element analyses consider material flow properties covering most structural and pressure vessel steels: $n = 5$ ($E/\sigma_0 = 800$), $n = 10$ ($E/\sigma_0 = 500$) and $n = 20$ ($E/\sigma_0 = 300$) with $E = 206$ GPa and $\nu = 0.3$; the stress-strain response for these materials is shown in Fig. 6. These ranges of properties also reflect the upward trend in yield stress with the decrease in strain hardening exponent characteristic of ferritic steels.

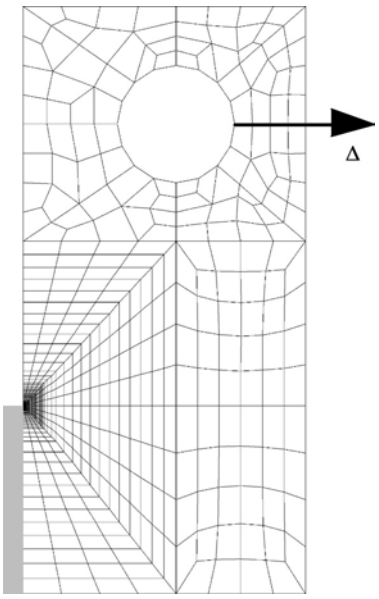

Figure 5. Plane-strain, finite element model for C(T) specimen with a/W=0.6 employed in the analyses.

Solution Procedures

The plane-strain analyses reported here are generated using the research code WARP3D (Koppenhoefer, 1994) which: (1) implements an incrementally-iterative Newton procedure to resolve the nonlinear equlibrium equations, (2) solves the equilibrium equations at each iteration using a very efficient, sparse matrix solver highly tuned for Unix and PC based architectures (3) evaluates the *J*-integral using a convenient domain integral procedure and (4) analyzes fracture models constructed with three-dimensional, 8-node tri-linear hexahedral elements. Use of the so-called formulation (Hughes, 1980) precludes mesh lock-ups that arise as the deformation progresses into fully plastic, incompressible modes. The sparse solver significantly reduces both memory and CPU time required for solution of the linearized equations compared to conventional direct solvers.

The local value of the mechanical energy release rate at a point along a crack front is given by (Rice, 1968)

$$J = \int_{\Gamma} \left[W n_1 - \sigma_{ij} \left(\partial u_i / \partial X_1 \right) n_j \right] d\Gamma \tag{9}$$

where Γ denotes a contour defined in a plane normal to the front on the undeformed configuration beginning at the bottom crack face and ending on the top face, n_j is the outward normal to Γ, W denotes the stress-work density per unit of undeformed volume, σ_{ij} and u_i are Cartesian components of stress and displacement in the crack front coordinate system. The finite element computations employ a domain integral procedure (Moran and Shih, 1987) for numerical evaluation of Eq. (9) computed over domains defined outside material having the highly non-proportional histories of the near-tip fields. Such *J*-values thus retain a strong domain (path) independence and agree with estimation schemes based upon eta-factors for deformation plasticity. They provide a convenient parameter to characterize the average intensity of far field loading on the crack front.

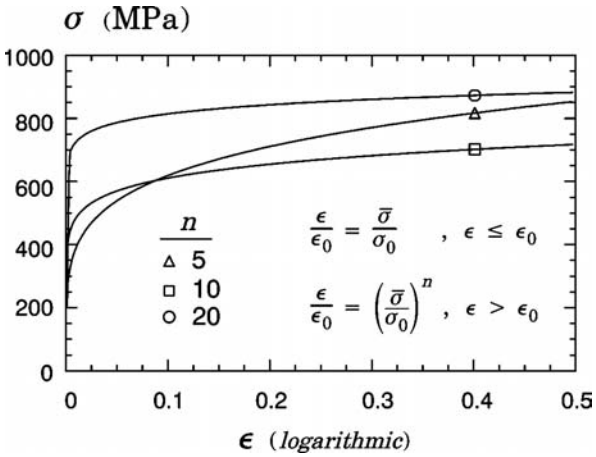

Figure 6. Stress-strain response for elastic-plastic materials employed in the analyses.

J-Q Trajectories for Fracture Specimens

This section describes results from detailed plane-strain analyses of C(T), SE(B), SE(T) and M(T) specimens to generate *J-Q* trajectories at locations ahead of crack tip. The approach to quantify the *Q*-levels in these finite cracked bodies utilizes full reference crack-tip fields constructed for the MBL model under SSY conditions shown in Fig. 2. The crack-tip fields computed for the fracture specimens are then compared to the SSY fields to evaluate Eq. (6) with increased loading as measured by *J*. The research code JQCRACK (Cravero and Ruggieri, 2002) is employed to compute *J-Q* curves for each fracture specimen.

Figures 8-10 provide key results which show the general effects of specimen geometry, loading mode and material properties on *J-Q* trajectories for the fracture specimens. In the plots, *Q* is defined by Eq. (6) at the normalized distance ahead of crack tip given by $r/(J/\sigma_0)=2$ whereas *J* is normalized by $b\sigma_0$ with *b* denoting the remaining crack ligament, *W–a* (notice that we plot $J/(b\sigma_0)$ *vs.* *–Q* to maintain positive scales). For each material (*n*=10 with $E/\sigma_0=500$; *n*=5 with $E/\sigma_0=800$ and *n*=20 with $E/\sigma_0=300$), the evolution of *Q* as loading progresses depends markedly on the specimen geometry. For the deep notch C(T) specimen in Figs. 8 and 9 (*n*=10 and *n*=5), the *Q*-parameter is positive at low load levels (which corresponds to positive elastic *T*-stresses for this geometry) and gradually change to negative values with increased levels of *J*. For this specimen with the low hardening material (*n*=20), *Q*-values are positive for the entire range of loading. In all these plots, the deep notch SE(B) and SE(T) specimens display a relatively similar behavior with comparable *J-Q* trajectories for almost the entire range of loading; this effect is more pronounced for the specimens with the low hardening material (*n*=20). In contrast, the deep notch M(T) specimen reveals large negative *Q*-values almost immediately upon loading for all strain hardening properties. Here, values for parameter *Q* ranging from –0.75 to –1.25 are associated with substantial reduction in the opening near-tip stresses for this specimen early in the loading.

Figure 11 provides additional results for the SE(B), SE(T) and M(T) fracture specimens showing the effect of crack size on *J-Q* trajectories for the material with *n*=10 and $E/\sigma_0=500$. The effect of a/W-ratio is especially prominent for the SE(B) and SE(T) specimens; *Q*-values for the $a/W=0.1$ configurations become highly negative upon initial loading. However, no such strong effect exists for the M(T) specimen; here, the *J-Q* trajectories display little sensitivity on the crack size.

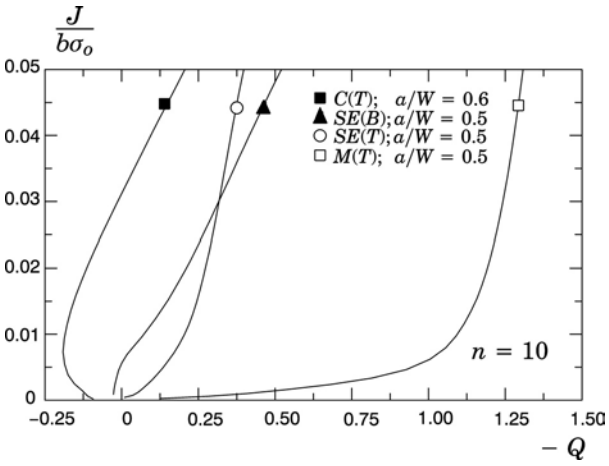

Figure 7. *J-Q* trajectories for deep notch specimens with *n=10*.

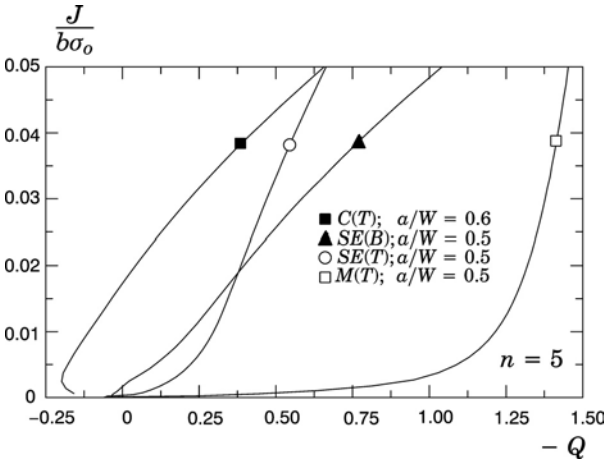

Figure 8. *J-Q* trajectories for deep notch specimens with *n=5*.

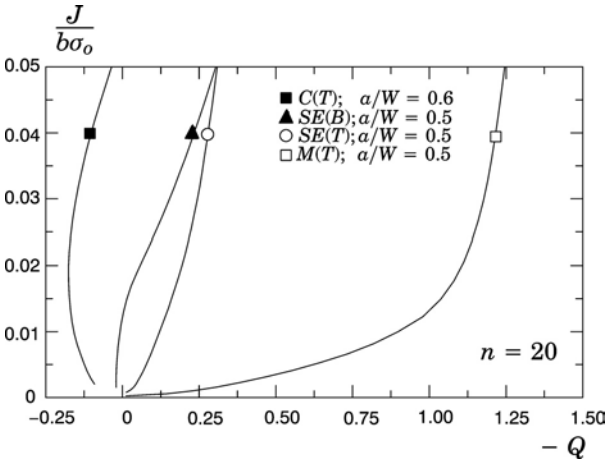

Figure 9. *J-Q* trajectories for deep notch specimens with *n=20*.

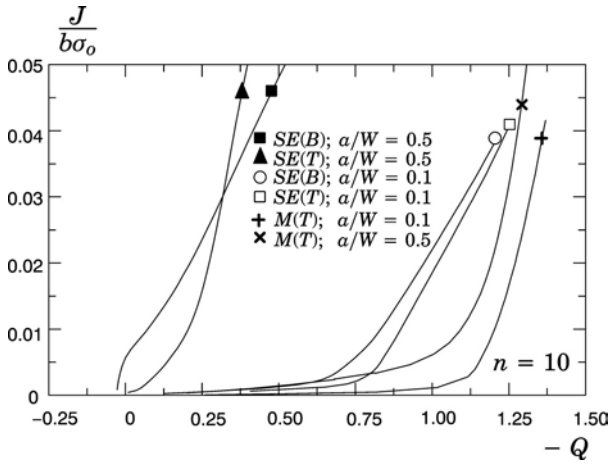

Figure 10. *J*-*Q* trajectories for the SE(B), SE(T) and M(T) specimens with *n*=10.

For convenience, the Q-values in the previous plots are computed at the particular distance $r=2(J/\sigma_0)$. Since Q is a measure of the deviation in the stress fields for the finite cracked body from the reference SSY fields, it is important to examine the variation of the difference parameter (Q) with crack-tip distance. Figures 12-18 shows Q-values computed at varying normalized distances, $1\leq r/(J/\sigma_0)\leq 5$, for all analyzed fracture specimens with n=10, E/σ_0=500 and increased deformation. Q-values for the deep notch C(T), SE(B) and SE(T) specimens displayed by the plots in Figs. 12, 16 and 18 show consistently increased radial dependence under increasing loading, particularly for large applied J-values. In contrast, Figs. 13-15 and 17 reveal that Q-values for the shallow notch SE(B) and SE(T) specimens and the M(T) specimen (a/W=0.1 and 0.5) are virtually independent of radial distance. This behavior merely reflects the interaction of the remote plastic bending field acting on the remaining ligament ($b=W-a$) with (local) crack-tip stresses, particularly at higher loads when large scale yielding develops. For the deep notch C(T), SE(B) and SE(T) specimens, the global bending field impinges strongly upon the crack tip resulting in lower near-tip stresses. For all shallow specimens and the M(T) specimen, this effect is much less pronounced even though Q takes on strong negative values upon initial loading.

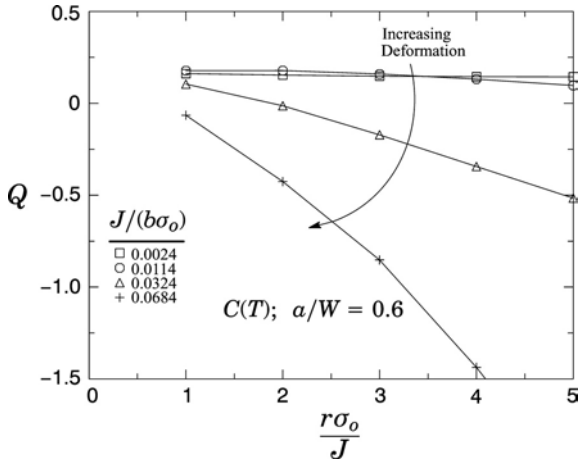

Figure 11. *Q* variation throughout the normalized radius for the C(T), a/w=0.6 specimen with *n*=10.

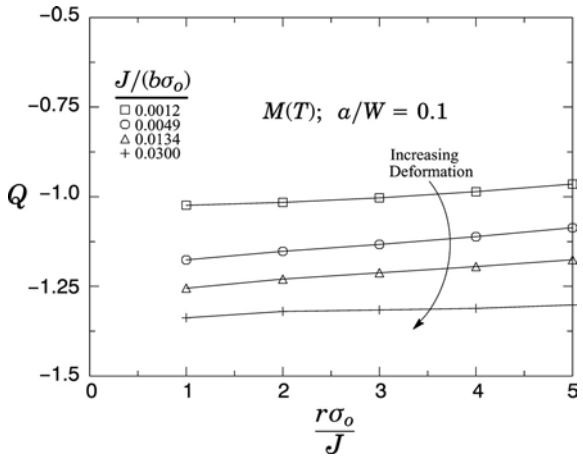

Figure 12. *Q* variation throughout the normalized radius for the M(T) a/w = 0.1 specimen with *n*=10.

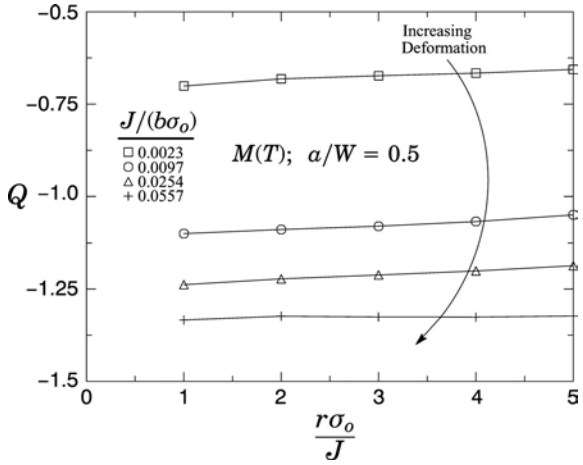

Figure 13. *Q* variation throughout the normalized radius for the M(T) a/w = 0.5 specimen with *n*=10.

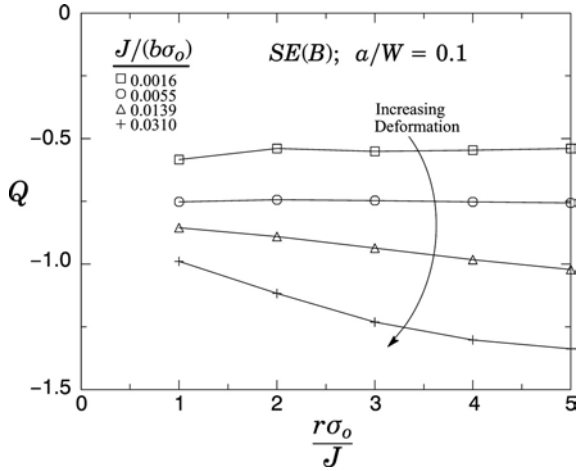

Figure 14. *Q* variation throughout the normalized radius for the SE(B) a/w = 0.1 specimen with *n*=10.

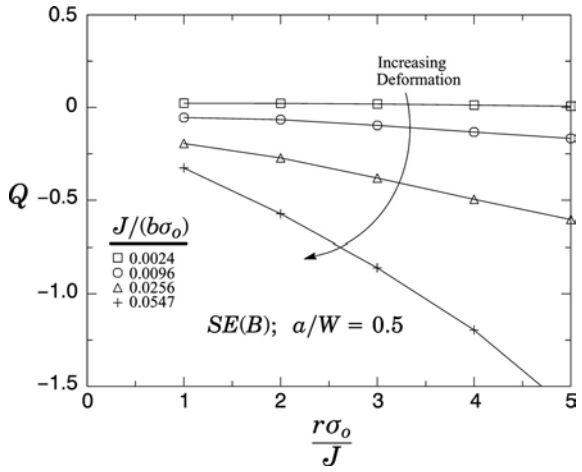

Figure 15. *Q* variation throughout the normalized radius for the SE(B) a/w = 0.5 specimen with *n*=10.

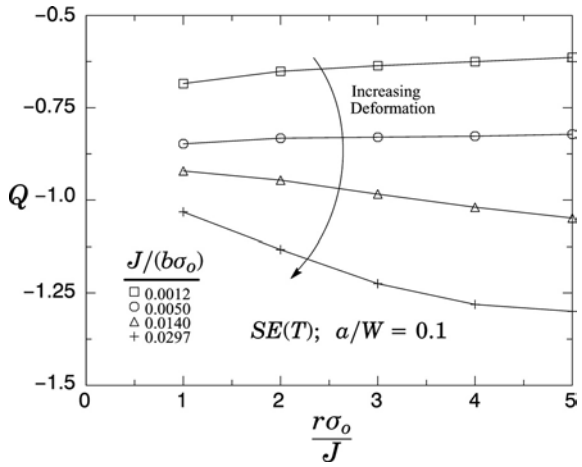

Figure 16. *Q* variation throughout the normalized radius for the SE(T) a/w = 0.1 specimen with *n*=10.

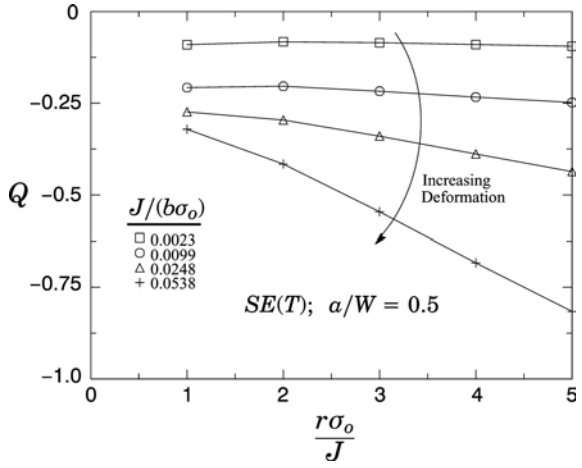

Figure 17. *Q* variation throughout the normalized radius for the SE(T) a/w = 0.5 specimen with *n*=10.

Constraint Effects on Cleavage Fracture

The previous *J-Q* trajectories provide a convenient description for the diverse range of crack-tip constraint under increased remote loading for cracked structural components. At low loads, the near-tip stresses and deformations evolve according to the self-similar SSY field characterized by high levels of stress triaxiality associated with low *Q*-values (either positive or negative values). As plastic flow progresses from well-contained yielding to large scale yielding, the near-tip stresses gradually relax below the levels for the high triaxiality SSY condition. This loss of crack-tip constraint is reflected by decreased values of *Q* for all fracture specimens, particularly for the shallow notch specimens and the M(T) specimen.

The features exhibited by the results displayed in Figs. 8-11 reveal important implications for fracture assessments of cracked components. Specifically, the levels of crack-tip constraint, conveniently quantified by *Q* within the present framework, affects strongly the brittle fracture process in ferritic materials. The role played by parameter *Q* can be explained in terms of the dependence of clevage fracture on critical levels of the near-tip opening stresses acting over microstructurally significant distances inside the fracture process zone (Ritchie et al., 1972). Negative *Q*-values lower the opening stresses ahead of crack tip which result in larger *J* values needed to trigger cleavage fracture. This is consistent with the observed effects of geometry and crack size on measured fracture toughness (see, for example, Fig. 1).

The characteristic trajectories for each fracture specimen displayed in Figs. 8-11 define the crack-tip driving force with increased loading in terms of (*J*, *Q*). Consequently, specimens with similar *J-Q* driving force curves should display similar fracture resistance behavior. In all plots, the deep notch C(T) specimen consistently exhibits higher levels of stress triaxiality than other deep notch specimens. For a given *a*/*W*-ratio, the SE(B) and SE(T) specimens have comparable levels of crack-tip constraint with increased loading. In contrast, however, *Q*-values for the deep and shallow notch specimens reveal a strong decrease in stress triaxiality almost immediately upon loading. Such features clearly emphasize the need of matching structural and test specimen constraint in fracture assessment procedures. Structural defects in engineering components are very often surface cracks that form during fabrication (*e.g.*, weld defects) or during in-service operation (*e.g.*, corrosion in oil and gas pipelines).These crack configurations generally develop low levels of crack-tip stress triaxiality which contrast sharply to conditions present in deeply cracked specimens commonly specified by test procedures to measure the cleavage fracture toughness of the material.

One application of the present two-parameter framework in fracture assessments involves the construction of *J-Q* toughness loci to characterize cleavage fracture resistance over a range of crack tip constraint at a fixed temperature in the DBT range. Experimentally measured *J*-values at cleavage fracture are plotted on the trajectories computed by finite element analyses for the specimens, such as those shown in Fig. 19(a). The *Q*-value at fracture is thus not measured; rather it is inferred by the *J* controlled location on the appropriate *J-Q* trajectory. The usual scatter in results observed for multiple tests of the same specimen configuration defines points that lie along the loading trajectory for that specimen. By connecting, separately, the upper-most fracture value on all loading trajectories tested and then the lower-most fracture values, measured envelopes of toughness may be constructed. The correlation of fracture conditions across different crack geometries/loading modes of the same material (and temperature) then proceeds without recourse to detailed features of the crack tip separation processes. At identical values of the scalar parameters (*J*, *Q*), the crack tip strain-stress fields that drive the local fracture process have identical values as well. Utilization of the toughness locus in fracture assessments is illustrated in Fig. 19(b). The driving force curve for a highly constrained geometry (structure A) rises rapidly in the *J-Q* space. Consequently, cleavage fracture occurs when it intersects the failure

locus for cleavage. In contrast, a low constraint geometry (structure B) induces a gradually rising driving force so that ductile tearing is the likely event at overload.

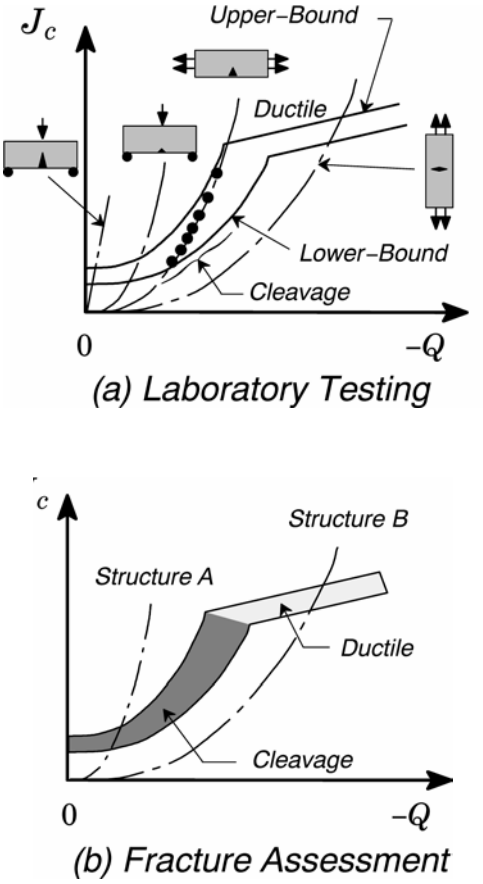

Figure 18. Application of a toughness locus based on the *J-Q* methodology in fracture assessments.

Concluding Remarks

The arguments presented in this brief paper, derived by extensive experimental observations, that conventional fracture mechanics approaches do not suffice to characterize the fracture behavior of fully yielded cracked solids provide compelling support to develop more realistic methodologies for fracture assessments. Our presentation explored the development and application of a descriptive approach employing the two-parameter characterization of crack-tip fields based upon on the *J-Q* theory.

Characterization of constraint effects on cleavage fracture toughness using parameters J and Q provides a basis for extending fracture mechanics methodology beyond the limits given by conditions pertaining to well-contained, near-tip plasticity. J sets the size scale of the zone of high stresses and large deformations while Q scales the near-tip stress level relative to a high triaxiality reference stress state. The present analyses show that the *J-Q* driving force curves suffice to quantify a wide range of near-tip constraint states at the onset of (cleavage) fracture.

Our results for a parameter study covering a broad range of material flow properties and varying constraint states associated with different fracture specimens convincingly demonstrate the strong effects of crack size and loading mode on the crack-tip driving forces. Such features clearly emphasize the need of matching constraint conditions present in defective structural components and test specimens employed in fracture assessment procedures. The representative plane-strain solutions presented in the paper demonstrate the utility and relative simplicity of this approach in describing cleavage fracture behavior under large scale yielding.

Because the *J-Q* correlative approach derives from a 2-D viewpoint, extension of the methodology within a 3-D framework appears essential to fully couple the microscale fracture process with global loading. However, inclusion of 3-D effects on *J-Q* trajectories required to obtain more accurate Q-values represents a much higher level of computational effort. Nevertheless, the present analyses do provide a more realistic and yet simpler procedure to assess constraint states in cracked bodies. On-going work addresses the development and design of test specimens specifically applicable to match the crack-tip constraint in longitudinally cracked pipelines under internal pressure.

Acknowledgements

This investigation is supported by Fundação de Amparo à Pesquisa do Estado de São Paulo (FAPESP) through Grant 01/06919-9 and through a graduate scholarship (02/06328-3) provided for the first author (SC). Funding to the second author (CR) is also provided by Conselho Nacional de Desenvolvimento Científico e Tecnológico (CNPq).

References

Al-Ani, A.M., and Hancock, J.W., 1991, "J-Dominance of Short Cracks in Tension and Bending", Journal of Mechanics and Physics of Solids, Vol. 39, pp. 23-43.

Betegon, C., and Hancock, J.W., 1991, "Two-Parameter Characterization of Elastic-Plastic Crack Tip Fields", ASME Journal of Applied Mechanics, Vol. 58, pp. 104-113.

Bilby, B.A., Cardew, G.E., Goldthorpe, M.R. and Howard, I.C., 1986, "Size Effects in Fracture", Institution of Mechanical Engineers, London, England, pp. 36-46.

Cravero, S., Ruggieri C., 2003, "JQCRACK Versão 1.0 Cálculo Numérico do Parâmetro Hidrostático Q para componentes Estruturais 2D Contendo Trinca." Boletim Técnico da Escola Politécnica da Universidade de São Paulo, Departamento de Engenharia Naval e Oceânica, BT/PNV/59.

Du, Z.-Z., and Hancock, J.W., 1991, "The Effect of Non-Singular Stresses on Crack-Tip Constraint", Journal of Mechanics and Physics of Solids, Vol. 39, pp. 555-567.

Hughes, T. J., 1980, "Generalization of Selective Integration Procedures to Anisotropic and Nonlinear Media", International Journal for Numerical Methods in Engineering, Vol. 15, pp. 1413-1418.

Hutchinson, J. W., 1968, "Singular Behavior at the End of a Tensile Crack in a Hardening Material", Journal of Mechanics and Physics of Solids, Vol.16, pp. 13-31.

Hutchinson, J.W., 1983, "Fundamentals of the Phenomenological Theory of Nonlinear Fracture Mechanics", ASME Journal of Applied Mechanics, Vol. 50, pp. 1042-1051.

Joyce, J. A. and Link, R. E., 1997, "Ductile-to-Brittle Transition Characterization Using Surface Crack Specimens Loaded in Combined Tension and Bending," in Fatigue and Fracture Mechanics: 28th Volume, ASTM STP 1321, J. H. Underwood, et al. Eds., American Society for Testing and Materials, Philadelphia, pp. 243-262.

Koppenhoefer, K., Gullerud, A., Ruggieri, C., Dodds, R. and Healy, B., 1994, "WARP3D: Dynamic Nonlinear Analysis of Solids Using a Preconditioned Conjugate Gradient Software Architecture", Structural Research Series (SRS) 596, UILU-ENG-94-2017, University of Illinois at Urbana-Champaign.

Larsson, S. G. and Carlsson, A. J., 1973, "Influence of Non-Singular Stress Terms and Specimen Geometry on Small Scale Yielding at Crack-Tip in Elastic-Plastic Materials", Journal of Mechanics and Physics of Solids, Vol.21., pp. 263-277.

Li, Y.C., and Wang, T.C., 1986, "Higher-Order Asymptotic Field of Tensile Plane-Strain Nonlinear Crack Problem", Scientia Sinica (Series A), Vol. 29, pp. 941-955.

Moran, B., and Shih, C.F., 1987, "A General Treatment of Crack Tip Contour Integrals", International Journal of Fracture, Vol. 35, pp. 295-310.

O'Dowd, N.P. and Shih, C.F., 1991, "Family of Crack-Tip Fields Characterized by a Triaxiality Parameter: Part I - Structure of Fields", Journal of the Mechanics and Physics of Solids, Vol. 39, pp. 989-1015.

O'Dowd, N.P. and Shih, C.F., 1992, "Family of Crack-Tip Fields Characterized by a Triaxiality Parameter: Part II - Fracture Applications", Journal of the Mechanics and Physics of Solids, Vol. 40, pp. 939-963.

Parks, D.M., 1992, "Advances in Characterization of Elastic-Plastic Crack-Tip Fields" in Topics in Fracture and Fatigue, A. S. Argon, Ed., Springer Verlag, pp. 59-98.

Rice, J., 1968, "A Path Independent Integral and the Approximate Analysis of Strain Concentration by Notches and Cracks," Journal of Applied Mechanics,Vol. 35, pp. 379-386.

Rice, J. R. and Rosengren, G. F., 1968, "Plane-Strain Deformation Near a Crack Tip in a Power-Law Hardening Material", Journal of Mechanics and Physics of Solids, Vol.16, pp. 1-12.

Rice, J. R., 1974, "Limitations to the Small Scale Yielding Approximation for Crack-Tip Plasticity", Journal of Mechanics and Physics of Solids, Vol.22, pp. 17-26.

Ritchie, R. O., Knott, J. F. and Rice, J. R., 1973, "On the Relationship Between Critical Tensile Stress and Fracture Toughness", Journal of the Mechanics and Physics of Solids, Vol. 21, pp. 395-410.

Ruggieri, C. and Dodds, R. H., 1996, "A Transferability Model for Brittle Fracture Including Constraint and Ductile Tearing Effects: A Probabilistic Approach", International Journal of Fracture, Vol. 79, pp. 309-340.

Sharma, S.M. and Aravas, N., 1991, "", Journal of Mechanics and Physics of Solids, Vol. 39, pp. 1043-1072.

Sorem, W.A., Dodds, R.H., and Rolfe, S.T., 1991, "Effects of Crack Depth on Elastic Plastic Fracture Toughness", International Journal of Fracture, Vol. 47, pp. 105-126.

Trovato, E. and Ruggieri, C., 2001, "Micromechanics Characterization of Constraint and Ductile Tearing Effects in Small Scale Yielding Fracture" International Journal of Solids and Structures, Vol. 38, pp. 2171-2187.

Wang, Y.Y., 1993, "On the Two-Parameter Characterization of Elastic-Plastic Crack-Front Fields in Surface-Cracked Plates" in Constraint Effects in Fracture, ASTM STP 1171, Hackett, et al. Eds., American Society for Testing and Materials, Philadelphia, pp. 120-138.

Williams, M. L., 1957, "On the Stress Distribution at the Base of a Stationary Crack", ASME Journal of Applied Mechanics, Vol. 24, pp. 109-114.